ECS Journal of Solid State Science and Technology, 2 (11) M44-M51 (2013)
2162-8769/2013/2(11)/M44/8/$31.00 © The Electrochemical Society

Effects of Propane/Nitrogen Mixtures on Thermal Chemical Vapor Deposition Rates and Microstructures of Carbon Films

Liang-Hsun Lai, Shao-En Chiou, Hsiang-Chun Hsueh, and Sham-Tsong Shiue[z]

Department of Materials Science and Engineering, National Chung Hsing University, Taichung 402, Taiwan

When propane/nitrogen (C_3H_8/N_2) mixtures are used to deposit carbon films by thermal chemical vapor deposition (CVD), effects of $C_3H_8/(C_3H_8+N_2)$ ratios on the deposition rate and microstructures of carbon films are investigated. Experimental results show that as the $C_3H_8/(C_3H_8+N_2)$ ratio increases from 20 to 100%, the deposition rate increases from 23.7 to 127 nm/min. Alternatively, if the residence time, deposition temperature, and working pressure raise, the deposition rate of carbon films also increases. The kinetics of this thermal CVD process is discussed. The activation energy obtained in this work is 234 kJ/mole. Furthermore, this CVD reaction is controlled by a process of about first order, which is resulted from the adsorption of main product gases, acetylene (C_2H_2) and ethylene (C_2H_4), on the silica glass plate substrate. Few nitrogen and hydrogen atoms are incorporated into carbon films. The crystallinity, ordering degree, and nano-crystallite size of carbon films decrease with increasing the $C_3H_8/(C_3H_8+N_2)$ ratio. Meanwhile, as the $C_3H_8/(C_3H_8+N_2)$ ratio increases from 20 to 100%, the $sp^2/(sp^2+sp^3)$ ratio of carbon films decreases from 92 to 61%. Finally, the results of thermal CVD carbon deposition using C_3H_8/N_2 mixtures are compared with those using methane/nitrogen (CH_4/N_2), C_2H_2/N_2, and C_2H_4/N_2 mixtures.
© 2013 The Electrochemical Society. [DOI: 10.1149/2.037311jss] All rights reserved.

Manuscript submitted August 16, 2013; revised manuscript received September 23, 2013. Published October 1, 2013.

Pyrolytic carbon is a kind of carbon materials that has been developed for a long time. The major use of pyrolytic carbon is in the form of coatings on substrates such as metals, ceramics, molded graphite, carbon foam, and carbon fibers.[1] For instance, pyrolytic carbon films have been formed by decomposing hydrocarbons in a heating reactor and depositing them on graphite particles[2,3] or optical fibers[4–7] using thermal chemical vapor deposition (CVD); such materials are also employed for graphite anodes in lithium ion secondary batteries[2,3] or as hermetic optical fiber coatings.[4–7] When carbon films are prepared by thermal CVD, their properties are affected by many factors such as the precursor gas, deposition temperature, working pressure, and mass flow rate of inlet gas.[2,3,6–8] Among the precursor gases, methane (CH_4) remains a popular choice because it is available in high purity.[7,9–12] Alternatively, acetylene (C_2H_2) is most used for low pressure deposition, because its C≡C bond has a simple dissociation pattern.[13] Nevertheless, the ordering degree of carbon films using C_2H_2 is lower, and the outlet of thermal CVD system is covered with contaminants including asphalts.[14,15]

Ethylene (C_2H_4) is an important product of petrochemical industry, and it is also often chosen as the precursor gas to prepare carbon films using different methods.[16–22] Alternatively, propane (C_3H_8) is clean, convenient, affordable, and effective, and thus, it is extensively used in the industrial, commercial, residential, and agricultural sectors.[23] Globally, C_3H_8 is the most widely used alternative vehicular fuel.[23] In the CVD method, C_3H_8 is adopted as the precursor gas to fabricate SiC thin films,[24] carbon nanotubes,[25] and graphene.[26] However, we found no reports from previous works concerning the influence of the propane/nitrogen (C_3H_8/N_2) mixture on the thermal CVD deposition rates and microstructures of carbon films. Hence, this study investigates the effects of the $C_3H_8/(C_3H_8+N_2)$ ratio on the thermal CVD deposition rates and microstructures of carbon films on silica glass plates. At a certain $C_3H_8/(C_3H_8+N_2)$ ratio, the effects of the mass flow rate of inlet gases, deposition temperature, and working pressure on the deposition rate are also studied. Furthermore, the kinetics of thermal CVD process and the connection between the microstructure of carbon films and thermal CVD process are proposed. Finally, the thermal CVD carbon deposition using a C_3H_8/N_2 mixture is compared with those using CH_4/N_2,[11] C_2H_2/N_2,[14] and C_2H_4/N_2 mixtures.[21]

Experimental

The preparation of carbon films proceeded as follows. The silica glass plates (length = 12 mm, width = 12 mm, and height = 1 mm) were subsequently cleaned in ultrasonic baths of acetone and deionized water to improve the adhesion of carbon films onto the substrates. Then, the silica glass plates were coated with carbon films by thermal CVD. The thermal CVD system adopted a quartz tube as the reaction chamber, which has a length of 900 mm, an internal diameter of 25 mm, and a wall thickness of 1.5 mm. The deposition zone length of the reaction chamber was 60 mm, and the substrate was placed in the reaction chamber so that the middle portion of the substrate's length coincides with that of the deposition zone. 99.9% C_3H_8 and 99.995% N_2 were used as the precursor gases. The total mass flow rates of C_3H_8 and N_2 were kept at 40 sccm (standard cubic centimeter per minute, cm^3/min), and five carbon films were prepared with the mass flow rates of C_3H_8 being 8, 16, 24, 32, and 40 sccm. This means that five carbon films were prepared with the $C_3H_8/(C_3H_8+N_2)$ ratios of 20, 40, 60, 80, and 100%. The working pressure was maintained at 40 ± 2 kPa by a mechanical pump. During the deposition process, a residual gas analyzer (Extorr-XT200M) was used to measure the partial pressures of the residual gases. After finishing the deposition process, the temperature of the deposition zone was quickly reduced to room temperature at a rate of 250 K/min by cooling in air with a fan.

In thermal CVD process, the deposition rate depends on not only the gas phase composition $C_3H_8/(C_3H_8+N_2)$ but also the mass flow rate (or residence time) of inlet gases, deposition temperature, and working pressure.[2,3,6–8] To understand the effects of the mass flow rate of inlet gases, deposition temperature, and working pressure on the deposition rate, other kinds of carbon films were prepared. In those cases, if the parameters were not specified, the $C_3H_8/(C_3H_8+N_2)$ ratio, total mass flow rate of C_3H_8 and N_2, deposition temperature, working pressure, and deposition time were set to 80%, 40 sccm, 1153 K, 40 kPa, and 10 min, respectively.

The thicknesses and morphologies of the carbon films were obtained by measuring the cross sections of the glass plate located at the middle position of the reactor using a field emission scanning electron microscope (FESEM, JEOL JSM-6700F). The operating voltage of the FESEM was 3 kV. The structural and chemical characterization of the carbon films were investigated by X-ray diffractometer (XRD, Bruker MXP-III), Raman scattering spectroscopy (Jobin Yvon Triax 550), and X-ray photoelectron spectroscopy (XPS, ULVAC-PHI PHI 1600 VersaProbe). All these experiments were done on carbon films located at the middle position of the reactor of the substrate. The XRD was performed using $Cu\ K_\alpha$ radiation (λ = 0.154 nm) in grazing incident diffraction mode, and the incident angle is 0.5 degrees. Diffraction peaks from the carbon films were discerned by 2θ angles ranging between 10 and 50 degrees. Data from the Joint Committee on Powder Diffraction Standards (JCPDS) database (Number: 75-1621) were used to identify the microstructure of the carbon films from the diffraction peaks.[27] XRD patterns were decomposed by Gaussian

[z]E-mail: stshiue@dragon.nchu.edu.tw

Downloaded on 2013-10-02 to IP 140.120.135.71 address. Redistribution subject to ECS license or copyright; see ecsdl.org/site/terms_use

functions, and a linear background has been considered. The peak of the silica glass substrate (amorphous SiO_2) was extracted from the XRD patterns to obtain the (002) peak of graphite. The Raman spectra (RS) were measured in back-scattering geometry with the 633 nm line of a He-Ne laser at room temperature in the spectral range of 800–2000 cm^{-1}. The laser power of the Raman scattering spectrometer was 25 mW, and a damper was adopted to weaken the laser power. When the irradiation time of the laser on the carbon films was set to 10 s/point, the surface morphologies of carbon films examined by optical microscope that showed no significant damage. The RS were also decomposed by Gaussian functions in order to examine its linear background. The photoelectron spectra of carbon films were acquired with $Mg\ K_\alpha$ radiation (photon energy = 1253.6 eV). All carbon core line (*C 1s*) spectra were acquired at the X-ray incident angle of 54 degrees. The pass energies for survey and *C KLL* scan are 117.0 and 23.6 eV, respectively. Moreover, the binding energy scale was calibrated using the *C 1s* core level of highly oriented pyrolytic graphite (HOPG) at 284.3 eV.

Deposition rate

Effects of $C_3H_8/(C_3H_8+N_2)$ *ratios.—* Figure 1 shows FESEM images of cross sections of the carbon films that are deposited on silica glass plates with different $C_3H_8/(C_3H_8+N_2)$ ratios. The thicknesses of carbon films are obtained by measuring cross sections of the silica glass plates located at the middle position of the reactor. The FESEM results show that the thicknesses of carbon films t_f are 237, 525, 793, 1121, and 1266 nm for the $C_3H_8/(C_3H_8+N_2)$ ratios being 20, 40, 60, 80, and 100%, respectively. Notably, each data of the film thickness was obtained from the average value of five different positions on the same specimen's cross section, and the standard deviation of the measured values was within 5%. This implies that the carbon films are uniformly deposited on silica glass plates. The deposition rate r_f of the carbon films can be calculated from the film thickness and deposition time. Figure 2a shows that the deposition rate r_f of carbon films on silica glass plates are 23.7, 52.5, 79.3, 112, and 127 nm/min for the

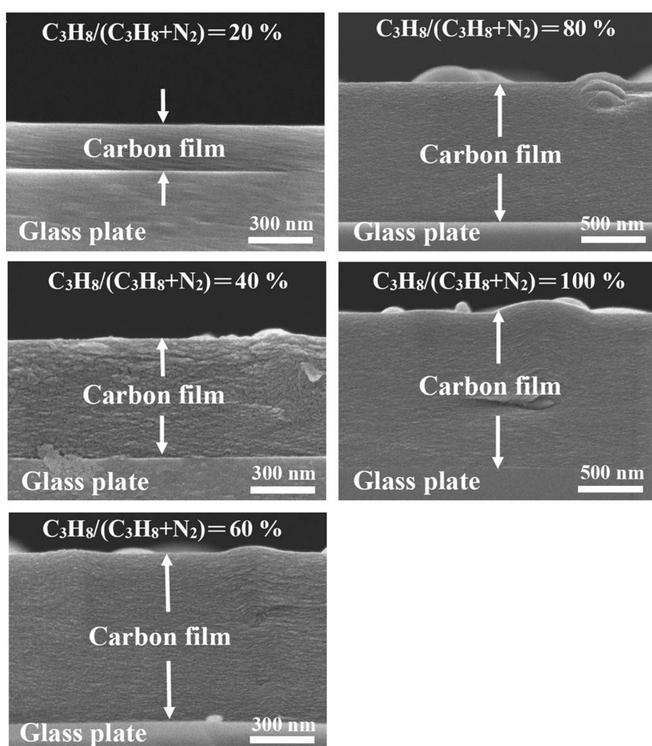

Figure 1. FESEM images of cross sections of carbon films deposited at different $C_3H_8/(C_3H_8+N_2)$ ratios.

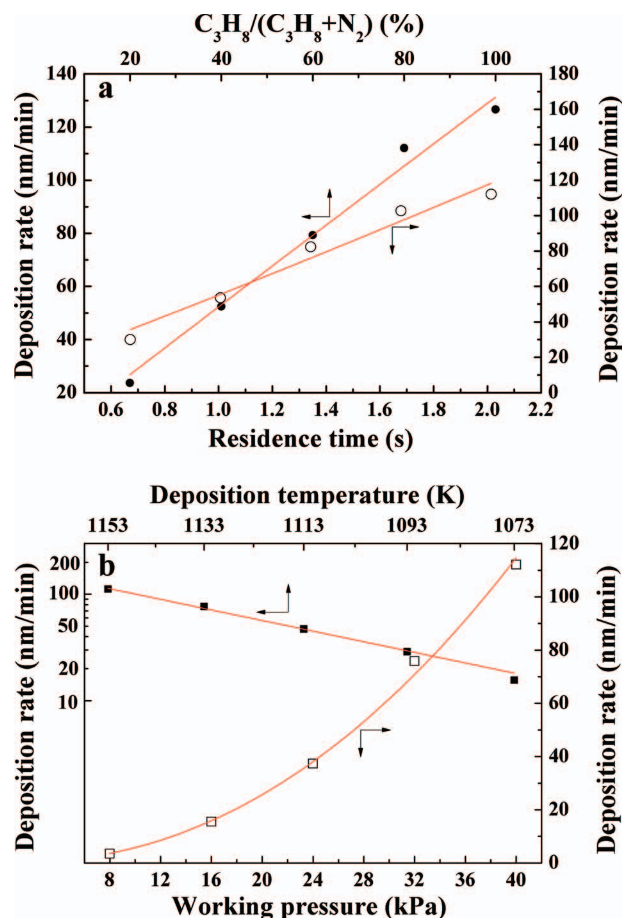

Figure 2. (a) The deposition rate of carbon films as a function of the $C_3H_8/(C_3H_8+N_2)$ ratio and residence time stayed at the deposition zone. (b) The dependence of the deposition rate of carbon films on the deposition temperature and working pressure.

$C_3H_8/(C_3H_8+N_2)$ ratios being 20, 40, 60, 80, and 100%, respectively. This indicates that the deposition rate of carbon films increases with increasing the $C_3H_8/(C_3H_8+N_2)$ ratio. The relation between the deposition rate of carbon films and the $C_3H_8/(C_3H_8+N_2)$ ratio can be further expressed by a power function as

$$r_f = k_1[(C_3H_8)/(C_3H_8 + N_2)]^n, \quad [1]$$

where k_1 and n are constants to be determined. After curve fitting using the data shown in Figure 2a, k_1 and n are obtained as 131 nm/min and 0.9, respectively. This indicates that this CVD reaction is controlled by a process of about first order. The details of residual gases analysis (RGA) results and kinetics of this thermal CVD process are described in Discussion and Appendix.

Figure 1 also illustrates that the carbon films exhibit a laminar structure. Pyrolytic carbon films prepared by thermal CVD usually exhibit a laminar structure.[28] Notably, when the $C_3H_8/(C_3H_8+N_2)$ ratio is above 60%, there appear many particles on the carbon-coated surface. The growth of these particles had been clearly described by Chen et al.[10] and Chen et al.[29]. Remarkably, the size and number of particles increase with the thickness of the carbon film, and thus, they also increase with the deposition rate and $C_3H_8/(C_3H_8+N_2)$ ratio. The laminar structure of the carbon film is disturbed by these particles, so the ordering degree of carbon coatings decreases.[10] Therefore, the ordering degree of the carbon films strongly depends on the particles on the carbon film surface.

Effects of total mass flow rates.— To understand the effect of the mass flow rate of inlet gases on the deposition rate, five carbon films

Table I. The film thickness t_f, deposition rate r_f, average flow velocity v_{av}, and residence time τ at various total mass flow rates of C_3H_8 and N_2.

Total mass flow rate of C_3H_8 and N_2 (sccm)	40	48	60	80	120
t_f (nm)	1121	1027	824	536	300
r_f (nm/min)	112	103	82.4	53.6	30.0
v_{av} (mm/s)	14.9	17.9	22.3	29.8	44.7
τ (s)	2.0	1.7	1.3	1.0	0.7

are prepared with the total mass flow rate of C_3H_8 and N_2 being 40, 48, 60, 80, and 120 sccm. In this case, the other unspecified process parameters are kept the same as those described in the experimental section. Table I shows that the deposition rates are 112, 103, 82.4, 53.6, and 30.0 nm/min for the total mass flow rates of C_3H_8 and N_2 being 40, 48, 60, 80, and 120 sccm, respectively. This indicates that the deposition rate decreases with increasing the total mass flow rate of C_3H_8 and N_2. The total mass flow rate of C_3H_8 and N_2 is related to the residence time, τ, of the precursor gas stayed in the deposition zone. Although the precursor gas is decomposed in the deposition zone, the relation between the total mass flow rate and residence time can be approximately estimated as follows. Based on the conservation of volume, the average flow velocity, v_{av}, of the precursor gas in the deposition zone can be obtained as $v_{av} = \dot{V}/(\pi d^2/4 - t \times w)$.[10,22] Here $\dot{V}$, d (= 25 mm), t (= 1 mm), and w (= 12 mm) are the volume flow rate, the internal diameter of the reactor, the thickness of the silica glass plate, and the width of the silica glass plate, respectively. Moreover, the volume flow rate $\dot{V}$ can be approximately obtained from the ideal gas equation as: $\dot{V} = \dot{n}RT/p$.[10,22] In this study, the working pressure p is 40 kPa; the gas constant R is 8.31 J/K · mole; the deposition temperature T is 1153 K, and $\dot{n}$ (mole/min) is the multiplication of 4.46×10^{-5} (mole/cm^3) and the total mass flow rate of C_3H_8 and N_2. Table I indicates that the average flow velocities, v_{av}, are 14.9, 17.9, 22.3, 29.8, and 44.7 mm/s for the total mass flow rates of C_3H_8 and N_2 being 40, 48, 60, 80, and 120 sccm, respectively. On the other hand, the length L of the deposition zone is 60 mm and the thickness of the carbon film was measured at the place located at the middle position of the reactor, and thus, the residence time, τ, of the precursor gas stayed in the deposition zone can be obtained as: $\tau = L/(2v_{av})$.[10,22] Table I also show that the residence times τ are 2.0, 1.7, 1.3, 1.0, and 0.7 s for the total mass flow rates of C_3H_8 and N_2 being 40, 48, 60, 80, and 120 sccm, respectively. Figure 2a also plots the relation between the deposition rate and residence time, indicating that the deposition rate increases with increasing the residence time. The dependence of the deposition rate on the residence time can be represented as:[10,22]

$$r_f = k_2[(\tau - \tau_c)/(\tau_0 - \tau_c)]^q, \quad [2]$$

where τ_0 (= 2.0 s) is the reference residence time. Notably, the deposition rate is relatively fast in this thermal CVD process, thus we assumed that the threshold residence time $\tau_c = 0$ s, and constants k_2 and q are obtained as 118 nm/min and 1.1, respectively, with an error within 10%.

Effects of deposition temperatures.— To understand the effect of the deposition temperature T on the deposition rate, five carbon films were prepared with the deposition temperatures of 1073, 1093, 1113, 1133, and 1153 K. In this case, the other unspecified process parameters are kept the same as those described in the experimental details.

Figure 2b shows that if the deposition temperatures are 1073, 1093, 1113, 1133, and 1153 K, the deposition rates are 15.6, 28.8, 47.1, 76.9, and 112 nm/min, respectively. This indicates that the dependence of the deposition rate on the deposition temperature follows the Arrhenius law. Hence, the constant k_1 in Eq. 1 can be replaced by

$$k_1 = k_0 \exp(-E/RT), \quad [3]$$

where E (= 234 kJ/mole) is the activation energy with a derivation within 10%, and $k_0 = 4.4 \times 10^{12}$ nm/min. Notably, as the temperature changes from 1073 to 1153 K, the residence time varies from 2.2 to 2.0 s. Because the variation of the residence times is small, we assume that the residence time is not changed here.

Effects of working pressures.— To further understand the effect of the working pressure on the deposition rate, five carbon films were prepared with the working pressures of 8, 16, 24, 32, and 40 kPa, where the derivation of working pressures is within 2 kPa. In this case, the other unspecified process parameters are kept the same as those described in the experimental details. Figure 2b reveals that if the working pressures are 8, 16, 24, 32, and 40 kPa, the deposition rates are 3.5, 15.5, 37.3, 75.9, and 112 nm/min, respectively. Notably, when the working pressure changes from 8 to 40 kPa, the residence time varies from 0.4 to 2.0 s. Therefore, the dependence of the deposition rate r_f on the working pressure p can be represented as:[22]

$$r_f = k_3[(\tau - \tau_c)/(\tau_0 - \tau_c)]^q[(p - p_c)/(p_0 - p_c)]^a, \quad [4]$$

where p_0 (= 40 kPa) is the reference working pressure. Moreover, the deposition rate is relatively fast in this thermal CVD process, thus we assumed that the threshold working pressure $p_c = 0$ kPa, and k_3 and a are constants to be determined. As stated above, the residence time τ in Eq. 4 is related to the working pressure p, and q (= 1.1), τ_0 (= 2.0 s) and τ_c (= 0 s) are constants. When the data of the deposition rates at various working pressures are substituted into Eq. 4, the constants k_3 and a are found to be 115 nm/min and 1.1, respectively, with an error well below 10%. The amount of C_3H_8 in the reaction gas not only is related to the $C_3H_8/(C_3H_8+N_2)$ ratio but also is proportional to the working pressure, and thus, the constant a is close to n in Eq. 1. Eqs. 1 and 4 show that the deposition rate is proportional to the partial pressure (or pressure) of C_3H_8 with a power of about first order, and thus, this CVD reaction is controlled by a process of about first order.

Structural and chemical characterization

Figure 3 shows XRD patterns of carbon films that are prepared with different $C_3H_8/(C_3H_8+N_2)$ ratios. This figure displays a diffraction peak around 20.8 degrees for the silica glass substrate and a (002) diffraction peak around 25.5 degrees for the graphite. The peak of silica glass substrate is extracted from the XRD pattern to obtain the

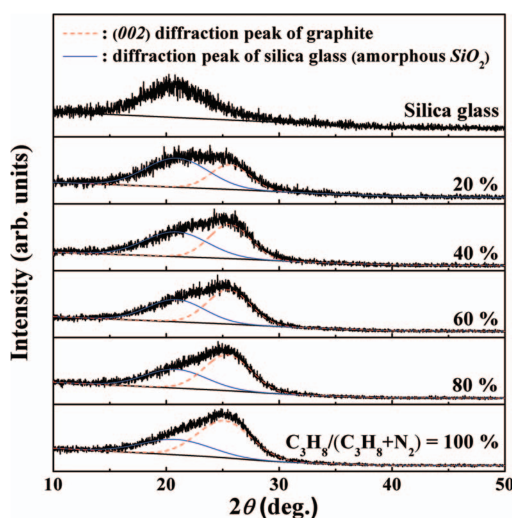

Figure 3. XRD patterns of carbon films deposited at different $C_3H_8/(C_3H_8+N_2)$ ratios. This figure reveals that XRD patterns include a (002) diffraction peak of graphite and a diffraction peak of silica glass.

(002) peak of the graphite. Moreover, to eliminate the intrinsic instrumental broadening, the B parameter was calculated using the equation, $B = (B_c^2 - B_{Si}^2)^{1/2}$, where B_c is the full-width-at-half-maximum (*FWHM*) of the (002) peak of the carbon films, and B_{Si} is the experimentally obtained *FWHM* of the (220) peak of a standard silicon sample.[30] Experimental results reveal that the diffraction angle of the (002) peak of the graphite, θ_B, decreases from 25.7 to 25.2 degrees as the $C_3H_8/(C_3H_8+N_2)$ ratio increases from 20 to 100%, while B_c of carbon films increases from 4.1 to 5.5 degrees. The increase of *FWHM* indicates that the crystallinity of carbon films decreases.[31] The mean crystallite size, L_c, of carbon films can be estimated using Scherrer's formula, $L_c = 0.9\lambda/(B \cos \theta_B)$, where λ (= 0.154 nm) is the wavelength of the copper K_α X-ray line.[31] The calculated result shows that the mean crystallite size (L_c) of carbon films decreases from 2.0 to 1.5 nm as the $C_3H_8/(C_3H_8+N_2)$ ratio increases from 20 to 100%. This also implies that the increase of the $C_3H_8/(C_3H_8+N_2)$ ratio raises the deposition rate of carbon films, but decreases the degree of ordering of carbon films.

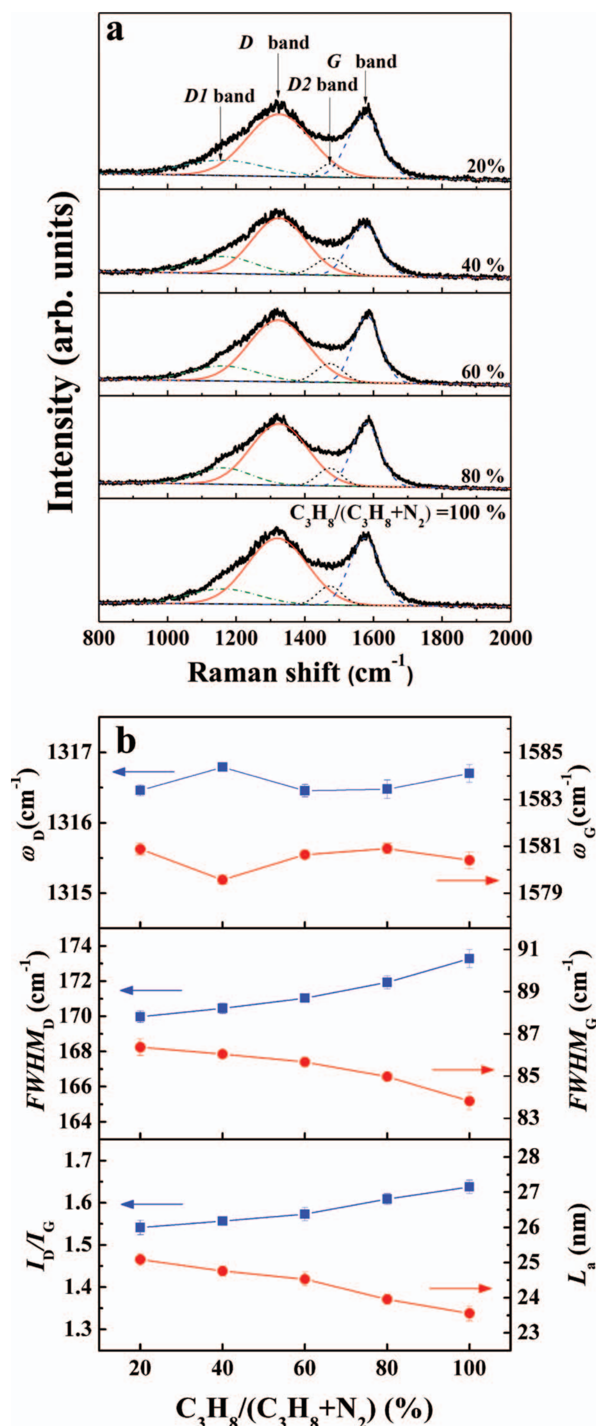

Figure 4. (a) Raman spectra of carbon films deposited at different $C_3H_8/(C_3H_8+N_2)$ ratios. The Raman spectra contain the D band at about 1350 cm^{-1}, G band at about 1580 cm^{-1}, $D1$ band at about 1200 cm^{-1}, and $D2$ band at about 1500 cm^{-1}. (b) Fitting results of Raman spectra and crystallite size L_a for carbon films deposited at different $C_3H_8/(C_3H_8+N_2)$ ratios.

Figure 4a shows RS of carbon films that are prepared with different $C_3H_8/(C_3H_8+N_2)$ ratios. The RS can be decomposed into four absorption peaks: D band at about 1350 cm^{-1}, G band at about 1580 cm^{-1}, $D1$ band at about 1200 cm^{-1}, and $D2$ band at about 1500 cm^{-1}. Here the D, G, $D1$, and $D2$ bands were fitted with Gaussian function, and this is suggested by Shimodaira et al.[32] The D band is associated with the breathing mode of sixfold sp^2 rings and identified as the disorder-activated band, this mode is forbidden in perfect graphite and only becomes active in the presence of disorder;[33] the G band is associated with the bond stretching vibrations of all sp^2 sites;[33] the $D1$ band is also related to the disorder graphitic lattice[33] but not uniquely defined,[34] and the $D2$ band is attributed to amorphous carbon.[35] Figure 4b shows the peak shift of the D band (ω_D) and G band (ω_G), the full-width-at-half-maximum of D band ($FWHM_D$) and G band ($FWHM_G$), and integrated intensity ratio of the D band to G band (I_D/I_G) for carbon films prepared with different $C_3H_8/(C_3H_8+N_2)$ ratios. This figure shows that as the $C_3H_8/(C_3H_8+N_2)$ ratio increases, ω_D and ω_G are slightly changed. Alternatively, this figure also reveals that as the $C_3H_8/(C_3H_8+N_2)$ ratio increases from 20 to 100%, $FWHM_D$ increases from 170 to 173 cm^{-1} and I_D/I_G values increase from 1.5 to 1.6. This indicates that the ordering degree of carbon films decreases with increasing the $C_3H_8/(C_3H_8+N_2)$ ratio.[33,34] The results also show that the $FWHM_G$ decreases from 86.4 to 83.8 cm^{-1} with increasing the $C_3H_8/(C_3H_8+N_2)$ ratio. The ratio of I_D and I_G is commonly used to approximately estimate the crystallite size of nanographite. Notably, I_D and I_G are the integrated intensities of the D band and G band, respectively. An expression that gives the crystallite size (L_a) from the integrated intensity ratio I_D/I_G is given by:[30] $L_a(nm) = (2.4 \times 10^{-10})\lambda_o^4(I_D/I_G)^{-1}$, where λ_o (= 633 *nm*) is the laser line wavelength used in the Raman experiment. This expression indicates that the crystallite size of nanographite increases with decreasing the I_D/I_G value. Hence, Figure 4b shows that when I_D/I_G values increase from 1.5 to 1.6 as the $C_3H_8/(C_3H_8+N_2)$ ratio increases from 20 to 100%, L_a decreases from 25.1 to 23.6 nm. The decrease of the crystallite size (L_a) of carbon films also indicates that the ordering degree of carbon films decreases.[33,34]

Figure 5 shows XPS spectra of carbon films that are prepared with the $C_3H_8/(C_3H_8+N_2)$ ratio equaling to 20%. This figure indicates that the *C 1s* core level around 285 eV and *O 1s* core level around 531 eV

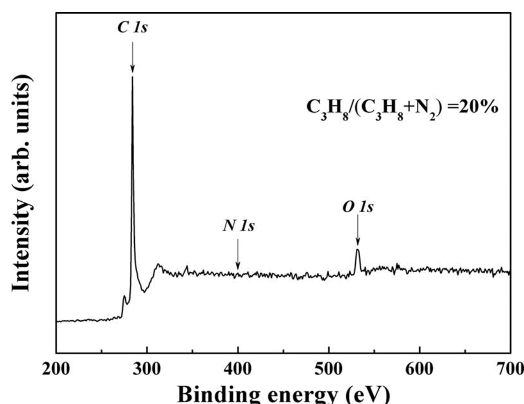

Figure 5. XPS spectrum of carbon film that is deposited with $C_3H_8/(C_3H_8+N_2) = 20\%$.

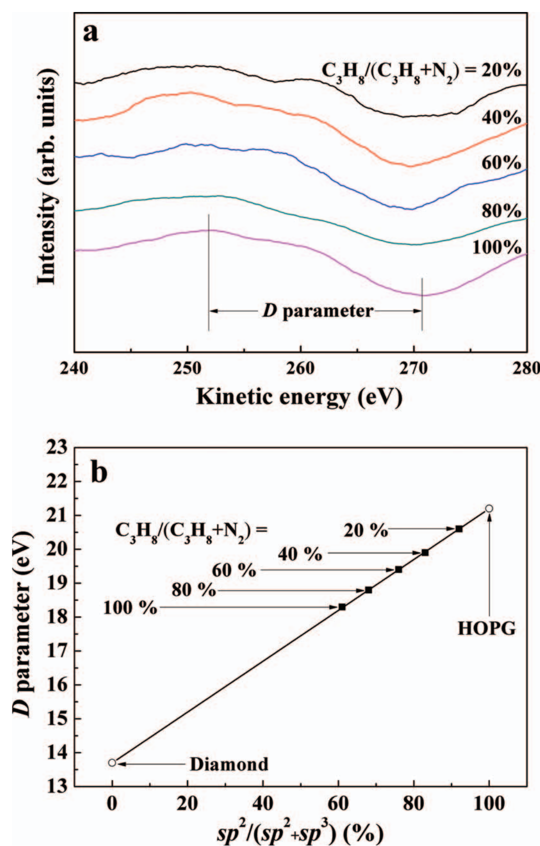

Figure 6. (a) First derivative *C KLL* spectra of carbon films deposited at different $C_3H_8/(C_3H_8+N_2)$ ratios. (b) Linear approximation of *D* parameters versus $sp^2/(sp^2+sp^3)$ ratios.

are revealed, but the *N 1s* core level around 400 eV is not found. The appearing of *O 1s* core level is assigned to atomic carbon bonded to surface adsorbents from the ambient.[36] Notably, XPS spectra of carbon films prepared with other $C_3H_8/(C_3H_8+N_2)$ ratios are not shown here, this is because they also only have the *C 1s* core level around 285 eV and *O 1s* core level around 531 eV. The analysis of sp^2/sp^3 ratios by decomposing the *C 1s* peak by Gaussian functions is a popular method, the peak area fractions of sp^2 and sp^3 carbon sites can be used to determine the sp^2/sp^3 ratio.[36–38] However, it is well-known that the determination of sp^2/sp^3 only on the basis of *C 1s* peak fitting does not seem a very reliable method and its validity should be thoroughly questioned.[39] To gain information on the contents of sp^2 and sp^3 carbon sites in the carbon film, X-ray-induced Auger peak of *C KLL* studies were carried out. It was noticed, that the peak-to-peak width of the main *C KLL* transition, which is easier to measure in the first derivative mode, is representing a fingerprint of the carbon states.[39–41] Later on, it was introduced a simplified method for analysis of the *C KLL* transition, which consists in the measurement of peak-to-peak width and applying its linear calibration from diamond to graphite.[42,43]

Figure 6a shows first derivative *C KLL* spectra of carbon films deposited at different $C_3H_8/(C_3H_8+N_2)$ ratios. The peak-to-peak width was named the D parameter of *C KLL* peak, and it was successfully used by numerous researchers for the determination of sp^2/sp^3 ratio in diamond-like carbon (DLC) films,[44,45] in multi-walled carbon nanotubes (MWCNTs),[46,47] and in nanodiamonds.[39,48–50]

The linear approximation of D parameters versus $sp^2/(sp^2+sp^3)$ ratios of carbon films was shown in Figure 6b. Figure 6b shows that the D parameters of the diamond and HOPG are 13.7 eV and 21.2 eV, respectively, and this is proposed by Mezzi and Kaciulis.[50] Meanwhile, it also reveals that the linearity of the D parameters versus $sp^2/(sp^2+sp^3)$ ratios between the diamond and graphite is confirmed

Table II. The *D* parameters and $sp^2/(sp^2+sp^3)$ ratios of carbon films analyzed by XPS at different $C_3H_8/(C_3H_8+N_2)$ ratios.

$C_3H_8/(C_3H_8+N_2)$ ratios (%)	20	40	60	80	100
D parameter (eV)	20.6	19.9	19.4	18.8	18.3
$sp^2/(sp^2+sp^3)$ (%)	92	80	76	68	61

by the experimental results. Moreover, Table II shows that the D value decreases from 20.6 to 18.3 as the $C_3H_8/(C_3H_8+N_2)$ ratio changes from 20 to 100%. The decrease in D value could be associated to the decreasing number of π electrons or sp^2 carbon sites in the film.[43] Moreover, Table II also shows that as the $C_3H_8/(C_3H_8+N_2)$ ratio changes from 20 to 100%, the $sp^2/(sp^2+sp^3)$ ratio of carbon films decreases from 92 to 61%.

Notably, RGA results (please see Discussion) reveal that the amounts of gas phase hydrogen increases with increasing the $C_3H_8/(C_3H_8+N_2)$ ratio. Sobol-Antosiak and Ptak[51] reported that the degree of surface hydrogen coverage tends to increase in nucleation processes, leading to the formation of carbon films, from gas phase by the CVD methods. The presence of hydrogen is considered to enhance the process of forming films with high sp^3 contribution. Consequently, the effect of gas phase hydrogen on the formation of carbon films may be taken to explain the reason why the sp^3 fraction in the carbon films increases with increasing the $C_3H_8/(C_3H_8+N_2)$ ratio. We had adopted Fourier transfer infrared (FTIR) spectroscope to measure the carbon films, and found that little hydrogen was within the carbon film. Hence, we can also predict that the *H* radicals were conjugated together to produce hydrogen gases, H_2, and then is also exhausted to the atmosphere.

Discussion

In this work, substrates are heated in a deposition reactor and well-mixed precursor gases are flowed through the reactor and heated up. After heated up in the deposition reactor, the precursor gas undergoes reactions in the gas phase. Simultaneously, complex heterogeneous reactions occur at the surface of the silica glass substrate. Deposition of the solid-phase carbon materials thus is a consequence of complex homogeneous gas-phase and heterogeneous surface reactions.[52] The RGA result reveals that the residual gases in the gas phase mainly contain H_2, CH_4, C_2H_2, C_2H_4, C_3H_8, and N_2; and also, some other

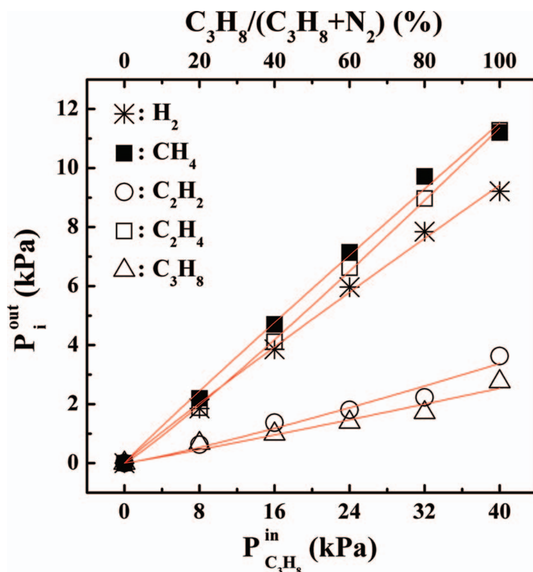

Figure 7. The partial pressures of the main residual gases as a function of the partial pressure of the inlet gas C_3H_8.

Table III. A comparison between the thermal CVD carbon deposition of this work and that of our previous works[11,14,21] at some specified process parameters.

	This work	Reference[11]	Reference[14]	Reference[21]
Precursor gas	C_3H_8 (32 sccm) N_2 (8 sccm)	CH_4(32 sccm) N_2 (8 sccm)	C_2H_2 (32 sccm) N_2 (8 sccm)	C_2H_4 (32 sccm) N_2 (8 sccm)
Deposition temperature (K)	1153	1248	1003	1033
Working pressure (kPa)	40	77	13.3	60
C/H ratio	3/8	1/4	1	1/2
Deposition rate (nm/min)	112	39.2	2.3	8.6
Activation energy (kJ/mole)	234	456	484	448
Power order of controlled process	about 1	1	5	2
Outlet Contaminants	Moderate	Small	Large	Moderate

secondary product gases CH_2, CH_3, C_2H_3, C_3H_3, C_3H_5, and C_6H_6. Notably, the partial pressures of the secondary product gases are much small than those of main gases, so only the latter gases are considered here. Remarkably, the RGA result shows that the partial pressure of the inlet gas N_2 is the same as that of the outlet gas N_2, so the N_2 gas is only used to reduce the partial pressure of C_3H_8.

Figure 7 shows the partial pressures of the main residual gases H_2, CH_4, C_2H_2, C_2H_4, and C_3H_8 at various partial pressures of the inlet gas C_3H_8. Notably, the partial pressures of the main residual gases H_2, CH_4, C_2H_2, C_2H_4, and C_3H_8 are denoted by $p^{out}_{H_2}$, $p^{out}_{CH_4}$, $p^{out}_{C_2H_2}$, $p^{out}_{C_2H_4}$, and $p^{out}_{C_3H_8}$, respectively; and the partial pressure of the inlet gas C_3H_8 is denoted by $p^{in}_{C_3H_8}$, which is the multiplication of the $C_3H_8/(C_3H_8+N_2)$ ratio and 40 kPa. The RGA result shows that $p^{out}_{H_2}$, $p^{out}_{CH_4}$, $p^{out}_{C_2H_2}$, $p^{out}_{C_2H_4}$, and $p^{out}_{C_3H_8}$ are proportional to $p^{in}_{C_3H_8}$. That are $p^{out}_{H_2} = b_0 p^{in}_{C_3H_8}$, $p^{out}_{CH_4} = b_1 p^{in}_{C_3H_8}$, $p^{out}_{C_2H_2} = b_2 p^{in}_{C_3H_8}$, $p^{out}_{C_2H_4} = b_3 p^{in}_{C_3H_8}$, and $p^{out}_{C_3H_8} = b_4 p^{in}_{C_3H_8}$, where $b_0 = 0.23$, $b_1 = 029$, $b_2 = 0.08$, $b_3 = 0.28$, and $b_4 = 0.07$. When the conversion of C_3H_8 into the product gases is a jth-order reaction, the rate equation can be expressed as: $d(p^{in}_{C_3H_8})/dt = -k_j(p^{in}_{C_3H_8})^j$, and thus, one obtains:

$$\left(p^{out}_{C_3H_8}\right)^{1-j} - \left(p^{in}_{C_3H_8}\right)^{1-j} = k_j(j-1)t_r, \quad [5]$$

where k_j is a constant and t_r is the residence time of the precursor gases stayed in the deposition zone. By substituting the data of $p^{out}_{C_3H_8}$ and $p^{in}_{C_3H_8}$ into Eq. 5, one obtains that $j = 1$. This means that the conversion of C_3H_8 to main product gases is a first-order reaction. Therefore, the dissociation of C_3H_8 may be represented by the following steps

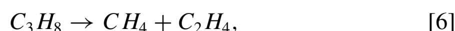

$$C_3H_8 \rightarrow CH_4 + C_2H_4, \quad [6]$$

and

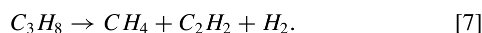

$$C_3H_8 \rightarrow CH_4 + C_2H_2 + H_2. \quad [7]$$

In this work, 99.9% C_3H_8 and 99.995% N_2 were used as the precursor gases, so the purities of the precursor gases may be too low. However, RGA results reveal that no unexpected impurities are found in the gas phase, and also, XPS results show that no unexpected impurities are observed in the carbon films. Therefore, we believe that no contamination occurs in the thermal CVD process.

The kinetics of this thermal CVD process is discussed, and the details are described in the Appendix. In brief, the precursor gases (C_3H_8 and N_2) are flowed through the reactor and heated up, and thus, some of precursor gases are decomposed. The deposition rate of carbon films is proportional to the partial pressure of the inlet gas C_3H_8 with a power of about first order, and the pyrolysis of C_3H_8/N_2 mixtures is resulted from the adsorption of the main product gases C_2H_2 and C_2H_4 on the silica glass plate substrate. The carbon species adsorbed on the substrate surface will further diffuse and conjugate to form the laminar graphite structure.[53]

The deposition of carbon films on the substrate needs adequate amount of carbon species in the gas phase (or sufficient residence time for carbon species to stay in the deposition zone). Hence, if the partial pressure (or working pressure) of C_3H_8 is smaller than the threshold pressure (or if the residence time is shorter than the threshold residence time), no film can be formed. However, in this thermal CVD process, the deposition rate is relatively fast, and thus, the threshold pressure and threshold residence time are zero. Moreover, as the residence time of the precursor gas stayed in the deposition zone increases, the amount of decomposed radicals also raises.[53] Consequently, the carbon fragment converted from these decomposed precursor gases to form carbon films on the substrate also increases.[53]

In our previous works, we adopted CH_4/N_2,[11] C_2H_2/N_2,[14] and C_2H_4/N_2[21] mixtures as the precursor gases to study the effects of deposition parameters on the properties of thermal CVD carbon films. A comparison between the results of this work and those of the previous works[11,14,21] at a specified process parameter is listed in Table III. Notably, the specified deposition parameters listed in Table III for various precursor gases are obtained by the authors to form a carbon film with smooth surface and good adhesion on the substrate surface, so they are different. The working pressure in previous work[14] was 13.3 kPa, but it was misprinted as 133 kPa. Table III shows that the deposition temperature of C_3H_8 (= 1153 K) is smaller than that of CH_4 (= 1248 K), but it is larger than those of C_2H_2 (= 1003 K) and C_2H_4 (= 1033 K). Alternatively, the working pressure of C_3H_8 (= 40 kPa) is smaller than those of CH_4 (= 77 kPa) and C_2H_4 (= 60 kPa), but it is larger than that of C_2H_2 (= 13.3 kPa). The hydrogen/carbon (*H/C*) ratio of C_3H_8 is 3/8, while the *H/C* ratios of CH_4, C_2H_4, and C_2H_2 are 1/4, 1/2, and 1, respectively. The deposition rate of C_3H_8 (= 112 nm/min) is larger than those of CH_4 (= 39.2 nm/min), C_2H_2 (= 2.3 nm/min), and C_2H_4 (= 8.6 nm/min), while the activation energy of C_3H_8 (= 234 kJ/mole) is lower than those of CH_4 (= 456 kJ/mole), C_2H_2 (= 484 kJ/mole), and C_2H_4 (= 448 kJ/mole). The pyrolysis of C_3H_8 with added N_2 is controlled by a process of about first-order; the pyrolysis of CH_4 with added N_2 is controlled by the first-order process; the pyrolysis of C_2H_2 with added N_2 is controlled by the fifth-order process, and the pyrolysis of C_2H_4 with added N_2 is controlled by the second-order process. As stated above, the pyrolysis of C_3H_8/N_2 mixtures is resulted from the adsorption of the main product gases C_2H_2 and C_2H_4 on the silica glass plate substrate. Because the deposition temperature of C_3H_8/N_2 is larger than those of C_2H_2/N_2 and C_2H_4/N_2, and thus, the deposition rate of C_3H_8/N_2 is larger than those of C_2H_2 and C_2H_4, while the activation energy of C_3H_8/N_2 is smaller than those of C_2H_2/N_2 and C_2H_4/N_2.[54] Moreover, it was found that the amount of contaminants in the outlet of thermal CVD system using CH_4 is small; the amount of contaminants in the outlet of thermal CVD system using C_3H_8 and C_2H_4 is moderate, and the amount of contaminants in the outlet of thermal CVD system using C_2H_2 is large.

Conclusions

When C_3H_8/N_2 mixtures are used to form carbon films by thermal CVD, effects of deposition parameters on the deposition rate and microstructures of carbon films are investigated. Experimental results show that as the $C_3H_8/(C_3H_8+N_2)$ ratio increases from 20 to 100%, the deposition rate increases from 23.7 to 127 nm/min. Alternatively, if the residence time, deposition temperature, and working pressure raise, the deposition rate of carbon films also increases. The deposition rate

of carbon films is proportional to the partial pressure of the inlet gas C_3H_8 with a power of about first order, and the pyrolysis of C_3H_8/N_2 mixtures is resulted from the adsorption of the main product gases C_2H_2 and C_2H_4 on the silica glass plate substrate. The activation energy obtained in this work is 234 kJ/mole. Few N and H atoms are incorporated into the carbon films. Because the deposition rate is relatively fast, the threshold pressure and the threshold residence time are zero. XRD results show that the crystallinity and mean crystallite size decrease with increasing the $C_3H_8/(C_3H_8+N_2)$ ratio. RS results show that the ordering degree and nano-crystallite size of carbon films decrease with increasing the $C_3H_8/(C_3H_8+N_2)$ ratio, this is because the size and number of particles in the carbon films increase. The RGA result shows that the partial pressure of the inlet gas N_2 is the same as that of the outlet gas N_2, so the N_2 gas is only used to reduce the partial pressure of C_3H_8. Alternatively, when the $C_3H_8/(C_3H_8+N_2)$ ratio increases, the hydrogen in the gas phase also increases, and thus, XPS results reveal that fraction of sp^3 carbon sites in carbon films raise. The results of this work are compared to those of using CH_4/N_2, C_2H_2/N_2, and C_2H_4/N_2 mixtures at a specified process parameter.

Acknowledgment

This work was supported by the National Science Council, Taiwan, under grant No. NSC 101-2221-E-005-031-MY2, and was also supported in part by the Ministry of Education, Taiwan, under the ATU plan.

Appendix A

Norinaga and Deutschmann[55] (also with their coworkers)[56] had investigated the detailed kinetic modeling of gas-phase reactions in the chemical vapor deposition of carbon from light hydrocarbons. Nevertheless, the RGA result of this study shows that the residual gases mainly include CH_4, C_2H_2, C_2H_4, and C_3H_8 species, so only these species will be supposed to be the main species able to adsorb at the deposition surface. Based on Langmuir-Hinshelwood kinetics,[57,58] we assume that the chemisorption of hydrocarbon species from the gas phase is irreversible, and the surface reactions by ring formation from carbon-hydrocarbon surfaces complexes are fast in comparison to hydrogen desorption; thus, only hydrogen desorption by back-formation of free sites is considered. The adsorption equilibria of chemisorbed hydrocarbon species and surface reactions of CH_4, C_2H_2, C_2H_4, and C_3H_8 species can be expressed as:

$$C_\infty(\,) + CH_4 \xrightarrow{k_{a1}} C_\infty(CH_4), \quad \text{[A1a]}$$

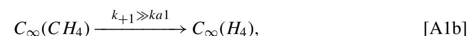

$$C_\infty(CH_4) \xrightarrow{k_{+1} \gg k_{a1}} C_\infty(H_4), \quad \text{[A1b]}$$

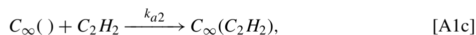

$$C_\infty(\,) + C_2H_2 \xrightarrow{k_{a2}} C_\infty(C_2H_2), \quad \text{[A1c]}$$

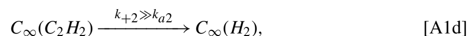

$$C_\infty(C_2H_2) \xrightarrow{k_{+2} \gg k_{a2}} C_\infty(H_2), \quad \text{[A1d]}$$

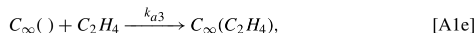

$$C_\infty(\,) + C_2H_4 \xrightarrow{k_{a3}} C_\infty(C_2H_4), \quad \text{[A1e]}$$

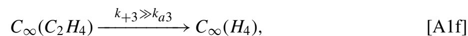

$$C_\infty(C_2H_4) \xrightarrow{k_{+3} \gg k_{a3}} C_\infty(H_4), \quad \text{[A1f]}$$

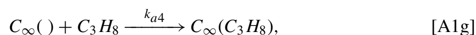

$$C_\infty(\,) + C_3H_8 \xrightarrow{k_{a4}} C_\infty(C_3H_8), \quad \text{[A1g]}$$

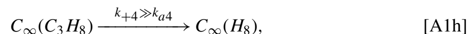

$$C_\infty(C_3H_8) \xrightarrow{k_{+4} \gg k_{a4}} C_\infty(H_8), \quad \text{[A1h]}$$

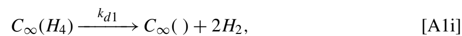

$$C_\infty(H_4) \xrightarrow{k_{d1}} C_\infty(\,) + 2H_2, \quad \text{[A1i]}$$

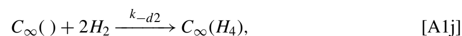

$$C_\infty(\,) + 2H_2 \xrightarrow{k_{-d2}} C_\infty(H_4), \quad \text{[A1j]}$$

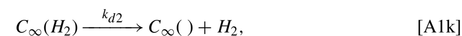

$$C_\infty(H_2) \xrightarrow{k_{d2}} C_\infty(\,) + H_2, \quad \text{[A1k]}$$

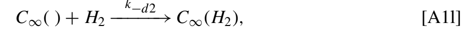

$$C_\infty(\,) + H_2 \xrightarrow{k_{-d2}} C_\infty(H_2), \quad \text{[A1l]}$$

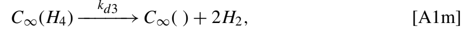

$$C_\infty(H_4) \xrightarrow{k_{d3}} C_\infty(\,) + 2H_2, \quad \text{[A1m]}$$

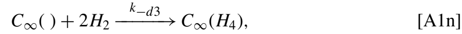

$$C_\infty(\,) + 2H_2 \xrightarrow{k_{-d3}} C_\infty(H_4), \quad \text{[A1n]}$$

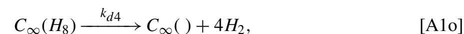

$$C_\infty(H_8) \xrightarrow{k_{d4}} C_\infty(\,) + 4H_2, \quad \text{[A1o]}$$

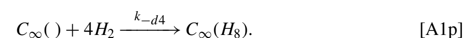

$$C_\infty(\,) + 4H_2 \xrightarrow{k_{-d4}} C_\infty(H_8). \quad \text{[A1p]}$$

Where $C_\infty(\,)$ = free active site; $C_\infty(CH_4)$, $C_\infty(C_2H_2)$, $C_\infty(C_2H_4)$, and $C_\infty(C_3H_8)$ = active sites with adsorbed hydrocarbon; $C_\infty(H_2)$, $C_\infty(H_4)$, and $C_\infty(H_8)$ = active sites with adsorbed hydrogen, and $k_{a1}, k_{+1}, k_{a2}, k_{+2}, k_{a3}, k_{+3}, k_{a4}, k_{+4}, k_{d1}, k_{-d1}, k_{d2}, k_{-d2}, k_{d3}, k_{-d3}, k_{d4}$, and k_{-d4} = rate constants.

The rate equations of above adsorption and desorption reactions can be expressed as:

$$r_{a1} = k_{a1} C_\infty(\,)\, p^{out}_{CH_4}, \quad \text{[A2a]}$$

$$r_{a2} = k_{a2} C_\infty(\,)\, p^{out}_{C_2H_2}, \quad \text{[A2b]}$$

$$r_{a3} = k_{a3} C_\infty(\,)\, p^{out}_{C_2H_4}, \quad \text{[A2c]}$$

$$r_{a4} = k_{a4} C_\infty(\,)\, p^{out}_{C_3H_8}, \quad \text{[A2d]}$$

$$r_{d1} = k_{d1} C_\infty(H) - k_{-d1} C_\infty(\,) p^{out}_{H_2}, \quad \text{[A2e]}$$

$$r_{d2} = k_{d2} C_\infty(H) - k_{-d2} C_\infty(\,) p^{out}_{H_2}, \quad \text{[A2f]}$$

$$r_{d3} = k_{d3} C_\infty(H) - k_{-d3} C_\infty(\,) p^{out}_{H_2}. \quad \text{[A2g]}$$

$$r_{d4} = k_{d4} C_\infty(H) - k_{-d4} C_\infty(\,) p^{out}_{H_2}. \quad \text{[A2h]}$$

The total concentration of active site, C, is the summation of that of free active site and active site with adsorbed hydrogen, that is

$$C = C_\infty(\,) + C_\infty(H). \quad \text{[A3]}$$

At steady-state conditions, the total adsorption rate is equal to the total desorption rate, and thus, we obtain

$$r_{a1} + r_{a2} + r_{a3} + r_{a4} = r_{d1} + r_{d2} + r_{d3} + r_{d4} = r_s, \quad \text{[A4]}$$

where r_s = pyrocarbon deposition rate, which is proportional to the deposition rate of the carbon film, r_f. Substituting Eqs. A2a–A2h and A3 into Eq. A4, one obtains

$$r_s = r_f/k_4 = \frac{C(k_{a1} p^{out}_{CH_4} + k_{a2} p^{out}_{C_2H_2} + k_{a3} p^{out}_{C_2H_4} + k_{a4} p^{out}_{C_3H_8})}{1 + [(k_{-d1} + k_{-d2} + k_{-d3} + k_{-d4}) p^{out}_{H_2} + (k_{a1} p^{out}_{CH_4} + k_{a2} p^{out}_{C_2H_2} + k_{a3} p^{out}_{C_2H_4} + k_{a4} p^{out}_{C_3H_8})]/(k_{d1} + k_{d2} + k_{d3} + k_{d4})}, \quad \text{[A5]}$$

where k_4 is a constant. We had adopted Fourier transfer infrared (FTIR) spectroscope to measure the carbon films, and found that little hydrogen was within the carbon film. Hence, we believe that the H radicals in the carbon film are desorbed. The desorbed H radicals may be conjugated together to produce hydrogen gases H_2, and then is exhausted to the atmosphere. And thus, RGA results show that there is a large amount of H_2 in the gas phase. Hence, we can predict that the rate constants of desorption, k_{d1}, k_{d2}, k_{d3}, and k_{d4} are much larger than that of adsorption. Accordingly, the second term on the denominator of Eq. A5 can be neglected. Therefore, Eq. A5 is reduced to:

$$r_f = k_4 C \left(k_{a1} p^{out}_{CH_4} + k_{a2} p^{out}_{C_2H_2} + k_{a3} p^{out}_{C_2H_4} + k_{a4} p^{out}_{C_3H_8} \right). \quad \text{[A6]}$$

Our experimental result shows that $k_{a2} p^{out}_{C_2H_2}$ and $k_{a3} p^{out}_{C_2H_4}$ are much larger than $k_{a1} p^{out}_{CH_4}$ and $k_{a4} p^{out}_{C_3H_8}$, and thus, Eq. A6 can be further reduced to:

$$r_f = k_4 C \left(k_{a2} p^{out}_{C_2H_2} + k_{a3} p^{out}_{C_2H_4} \right). \quad \text{[A7]}$$

Because $p^{out}_{C_2H_2} = b_2 p^{in}_{C_3H_8}$ and $p^{out}_{C_2H_4} = b_3 p^{in}_{C_3H_8}$, so Eq. A7 can be rearranged as:

$$r_f = k_4 C (k_{a2} b_2 + k_{a3} b_3) p^{in}_{C_3H_8}. \quad \text{[A8]}$$

As compared to Eq. 1, we find that $k_4 C(k_{a2} b_2 + k_{a3} b_3) = k_1/40kPa$. As stated in Eqs. 1 and 4, the deposition rate of carbon films is proportional to the partial pressure of the inlet gas C_3H_8 with a power of about first order, and thus, the pyrolysis of C_3H_8 with added N_2 is resulted from the adsorption of the main product gases C_2H_2 and C_2H_4 on the silica glass plate substrate. Remarkably, the rate constants k_{a2} and k_{a3} in Eq. A8 are related to the residence time $(\tau-\tau_c)/(\tau_0-\tau_c)$ in Eq. 2 and the temperature $\exp(-E/RT)$ in Eq. 3. The total concentration of active sites C in Eq. A8 is dependent on the specific surface area of the substrate. In this study, the substrate is not changed, so C is a constant. Furthermore, the carbon species adsorbed on the substrate surface will further diffuse and conjugate to form the laminar graphite structure.[53]

References

1. H. O. Pierson, *Handbook of Carbon, Graphite, Diamond and Fullerenes: Properties, Processing and Applications,* Noyes Publications, New Jersey (1995).
2. Y. S. Han and J. Y. Lee, *Electrochim. Acta*, **48**, 1073 (2003).
3. Y. S. Ding, W. N. Li, S. Iaconetti, X. F. Shen, J. DiCarlo, F. S. Galasso, and S. L. Suib, *Surf. Coat. Technol.*, **200**, 3041 (2006).
4. N. Yoshizawa, H. Tada, and Y. Katsuyama, *J. Lightwave Technol.*, **9**, 417 (1991).
5. S. T. Shiue, *J. Appl. Phys.*, **85**, 3044 (1999).
6. C. A. Taylor and W. K. S. Chiu, *Surf. Coat. Technol.*, **168**, 1 (2003).
7. S. S. Chen, S. T. Shiue, Y. H. Wu, and K. J. Cheng, *Surf. Coat. Technol.*, **202**, 798 (2007).
8. W. N. Li, Y. S. Ding, S. L. Suib, J. F. DiCarlo, and F. S. Galasso, *Surf. Coat. Technol.*, **190**, 366 (2005).
9. A. Grill, *Diam. Relat. Mater.*, **8**, 428 (1999).
10. P. Y. Chen, S. T. Shiue, and H. Y. Lin, *Thin Solid films*, **518**, 2883 (2010).
11. S. T. Shiue, P. Y. Chen, R. H. Lee, T. S. Chen, and H. Y. Lin, *Surf. Coat. Technol.*, **205**, 780 (2010).
12. C. Y. Lin, L. H. Lai, Y. X. Liu, S. T. Shiue, and H. Y. Lin, *J. Electrochem. Soc*., **158**, D445 (2011).
13. R. Kleber, M. Weiler, A. Kruger, S. Sattel, G. Kunz, K. Jung, and H. Ehrhardt, *Diam. Relat. Mater.*, **2**, 246 (1993).
14. R. H. Lee, L. H. Lai, and S. T. Shiue, *Thin Solid Films*, **518**, 7267 (2010).
15. L. H. Lai and S. T. Shiue, *Surf. Coat. Technol.*, **215**, 161 (2013).
16. S. Pirzada, J. J. Liu, F. Li, B. Demczyk, and D. Spaulding, *J. Appl. Phys.*, **91**, 7562 (2002).
17. M. Umeno and S. Adhikary, *Diam. Relat. Mater.*, **14**, 1973 (2005).
18. D. C. Ghimire, S. Adhikari, H. R. Aryal, S. M. Mominuzzamn, T. Soga, T. Jimbo, H. Uchida, and M. Umeno, *Diam. Relat. Mater.*, **17**, 1724 (2008).
19. O. Guise, H. Marbach, J. Levy, J. Ahner, and J. T. Yates Jr., *Surf. Sci.*, **571**, 128 (2004).
20. J. Niu, L. Zhang, Z. Zhang, D. Liu, Y. Liu, and Z. Feng, *Appl. Surf. Sci.*, **256**, 6887 (2010).
21. L. H. Lai, K. J. Huang, S. T. Shiue, J. T. Chang, and J. L. He, *J. Electrochem. Soc.*, **159**, D367 (2012).
22. L. H. Lai, H. C. Li, S. T. Shiue, T. J. Yang, and H. Y. Lin, *ECS J. Solid State Sci. Technol.*, **2**, N80 (2013).
23. M. Rood Werpy, A. Burnham, and K. Bertram, *Propane vehicles : status, challenges, and opportunities*, Argonne National Laboratory (ANL), Chicago, 2010. (http://www.ipd.anl.gov/anlpubs/2010/06/67243.pdf).
24. B. Shi, X. C. Liu, M. X. Zhu, J. H. Yang, and E. W. Shi, *Appl. Surf. Sci.*, **259**, 685 (2012).
25. J. Sengupta and C. Jacob, *J. Nanosci. Nanotechno.*, **10**, 3064 (2010).
26. J. K. Wassei, M. Mecklenburg, J. A. Torres, J. D. Fowler, B. C. Regan, R. B. Kaner, and B. H. Weiller, *Small*, **8**, 1415 (2012).
27. D. Yuan, J. Zeng, J. Chen, S. Tan, Y. Liu, N. Kristian, and X. Wang, *J. Electrochem. Soc.*, **156**, B377 (2009).
28. X. Bourrat, J. Lavenac, F. Langlais, and R. Naslain, *Carbon*, **39**, 2376 (2001).
29. S. S. Chen, S. T. Shiue, K. J. Cheng, P. Y. Chen, and H. Y. Lin, *Opt. Eng.*, **47**, 045005-1 (2008).
30. L. G. Cancado, K. Takai, T. Enoki, M. Endo, Y. A. Kim, H. Mizusaki, A. Jorio, L. N. Coelho, R. Magalhães-Paniago, and M. A. Pimenta, *Appl. Phys. Lett.*, **88**, 163106-1 (2006).
31. B. D. Cullity and S. R. Stock, *Elements of X-ray Diffraction*, third ed., Prentice Hall, New Jersey (2001).
32. N. Shimodaira and A. Masui, *J. Appl. Phys*, **92**, 902 (2002).
33. A. C. Ferrari and J. Robertson, *Phys. Rev. B*, **61**, 14095 (2000).
34. A. C. Ferrari and J. Robertson, *Phys. Rev. B*, **63**, 121405-1 (2001).
35. A. Sadezky, H. Muckenhuber, H. Grothe, R. Niessner, and U. Poschl, *Carbon*, **43**, 1731 (2005).
36. H. S. Zhang and K. Komvopoulos, *J. Appl. Phys.*, **106**, 093504-1 (2009).
37. P. Mérel, M. Tabbal, M. Chaker, S. Moisa, and J. Margot, *Appl. Surf. Sci.*, **136**, 105 (1998).
38. G. L. Dû, N. Celini, F. Bergaya, and F. Poncin-Epaillard, *Surf. Coat. Technol.*, **201**, 5815 (2007).
39. S. Kaciulius, *Surf. Interface. Anal.*, **44**, 1155 (2012).
40. Y. Mizokawa, T. Miyasato, S. Nakamura, K. M. Geib, and C. W. Wilmsen, *Surf. Sci.*, **182**, 431 (1987).
41. Y. Mizokawa, T. Miyasato, S. Nakamura, K. M. Geib, and C. W. Wilmsen, *J. Vac. Sci. Technol., A*, **5**, 2809 (1987).
42. J. C. Lascovich and S. Scaglione, *Appl. Surf. Sci.*, **78**, 17 (1994).
43. J. C. Lascovich, R. Giorgi, and S. Scaglione, *Appl. Surf. Sci.*, **47**, 17 (1991).
44. A. De Bonis, J. V. Rau, A. Santagata, and R. Teghil, *Surf. Coat. Technol.*, **205**, 3747 (2011).
45. J. V. Rau, R. Teghil, A. De Bonis, A. Generosi, B. Paci, R. Generosi, M. Fosca, D. Ferro, V. Rossi Albertini, and N. S. Chilingarov, *Diam. Relat. Mater.*, **19**, 7 (2010).
46. B. Lesiak, J. Zemek, P. Jiricek, L. Stobinski, and A. Jozwik, *Phys. Stat. Sol. B*, **247**, 2838 (2010).
47. L. Stobinski, B. Lesiak, L. Köver, J. Tóth, S. Biniak, G. Trykowski, and J. Judek, *J. Alloys Comp.*, **501**, 77 (2010).
48. F. Y. Xie, W. G. Xie, L. Gong, W. H. Zhang, S. H. Chen, Q. Z. Zhang, and J. Che, *Surf. Interf. Anal.*, **42**, 1514 (2010).
49. L. Constant and F. Le Normand, *Thin Solid Films*, **516**, 691 (2008).
50. A. Mezzi and S. Kaciulis, *Surf. Interface. Anal.*, **42**, 1082 (2010).
51. J. Sobol-Antosiak and W. S. Ptak, *Mater. Lett.*, **56**, 842 (2002).
52. K. J. Hüttinger, *Chem. Vapor. Depos.*, **4**, 151 (1998).
53. A. Becker and K. J. Huttinger, *Carbon*, **36**, 213 (1998).
54. L. S. Kershenbaum and J. Martin, *A. I. Ch. E. Journal*, **13**, 148 (1967).
55. K. Norinaga and O. Deutschmann, *Ind. Eng. Chem. Res.*, **46**, 3547 (2007).
56. K. Norinaga, O. Deutschmann, N. Saegusa, and J. I. Hayashi, *J. Analytical Appl. Pyrolysis*, **86**, 148 (2009).
57. G. F. Froment and K. B. Bischoff, *Chemical Reactor Analysis and Design*, John Wiley & Sons, New York (1979).
58. K. Norinaga and K. J. Huttinger, *Carbon*, **41**, 1509 (2003).